Nuclear import and chaperoning of monomeric histones H3 and H4 is mediated by Imp5, NASP and the HAT1 complex

Alonso J. Pardal and Andrew J. Bowman*

Biomedical Sciences, Warwick Medical School, University of Warwick, Gibbet Hill Road, Coventry, CV4 7AL, UK

Graphical Abstract

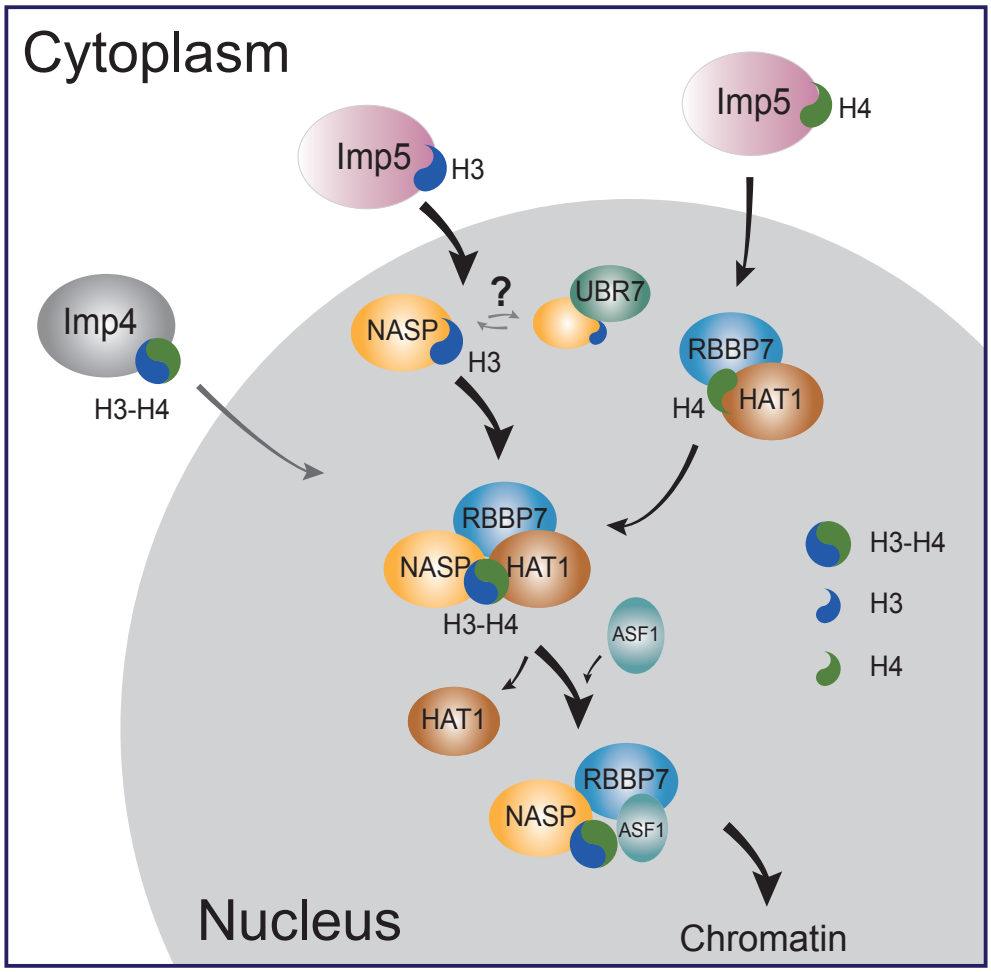

*Corresponding author: a.bowman.1@warwick.ac.uk

Abstract

Core histones package chromosomal DNA and regulate genomic transactions, with their import and deposition involving a dedicated repertoire of molecular chaperones. Histones H3 and H4 have been predominantly characterised as obligate heterodimers, however, recent findings have alluded to the existence of a significant pool of monomeric histone H3 in the nucleoplasm. Using a combination of *in vitro* and *in vivo* experiments, here we show that monomeric H3 and H4 use an Importin 5 (Imp5) dependent pathway for their nuclear import, distinct from Importin 4 (Imp4) previously described for H3-H4 dimers. Using mutants that disrupt the histone fold, we show monomeric H3 loses its interaction with Imp4, but retains interactions with Imp5 and the chaperone NASP. H4 monomeric mutants similarly bind Imp5 and not Imp4, however, they lose interaction with NASP, retaining their interaction with the HAT1-RBBP7 complex instead. *In vitro* experiments revealed that Imp5 and NASP are mutually exclusive in their binding, suggesting a facilitated hand-off mechanism. Furthermore, new H3 accumulates rapidly in a NASP-bound complex after nuclear translocation. NASP can assemble into three distinct co-chaperoning complexes, including a novel complex containing NASP, H3 and the putative ubiquitin ligase UBR7, a NASP-H3-H4-RBBP7 subcomplex and the previously characterised NASP-H3-H4-ASF1-HAT1-RBBP7 multi-chaperoning complex. Here we propose an alternative import pathway and folding mechanism for monomeric H3 and H4 that involves Imp5, rather than Imp4, and hands off to nuclear chaperones NASP, RBBP7 and HAT1.

Introduction

Chromatin is composed of an array of proteins and genomic DNA whose integrity is crucial for genomic regulation, stability, replication and repair. Histones are among the most abundant nuclear proteins, functioning in both packaging and regulation of access to DNA. Mechanisms by which histones are imported, chaperoned and deposited onto DNA are therefore of great current interest. The histone-fold dimers H3-H4 and H2A-H2B, which form the nucleosome core particle, have distinct import and chaperoning factors. Most of the current evidence indicates that both H3-H4 and H2A-H2B dimerise rapidly in the cytoplasm after synthesis and are imported in their dimeric state (Groth et al., 2005; Tagami et al., 2004; Campos and Reinberg, 2010; Yoon et al., 2018; Mosammaparast et al., 2002, 2001). However, recent observations using pulse-chase analysis alluded to the nuclear import of monomeric H3 and H4, pointing towards the existence of other pathways for nuclear import (Apta-Smith et al., 2018).

Histones are synthesised in the cytoplasm and translocate to the nucleus associated with importin proteins (also known as karyopherins). Once in the nucleus, importins interact with RanGTP leading to the unloading of their cargo and export to the cytoplasm (Chook and Süel, 2011). Karyopherin subunit β1 (KPNB1) binds to Nuclear Localisation Signals (NLS) via importin-α adaptor proteins. However, many nuclear proteins do not present a canonical NLS but rely on an extended importin-β family for direct binding and translocation (Muhlhausser et al., 2001; Soniat et al., 2016; Bernardes and Chook, 2020). Work on different organisms has cemented the notion that, despite certain redundancy, most importin-histone interactions are specific (Baake et al., 2001; Muhlhausser et al., 2001; Mosammaparast et al., 2001, 2002; Blackwell Jr. et al., 2007). For instance, in humans, nuclear import of histone H3-H4 dimers is associated with Imp4, and to a lesser extent, Imp5 and KPNB1 (Campos and Reinberg, 2010; Campos et al., 2015; Alvarez et al., 2011), whilst histones H2A and H2B mainly associate with importin-9 (Imp9), (Padavannil et al., 2019).

Histone chaperones also associate promptly with nascent histones, providing an environment for solubility and ensuring correct folding before targeting towards sites of DNA deposition (Hammond et al., 2017; Pardal et al., 2019). Nuclear Autoantigenic Sperm Protein (NASP) was first identified as an H1-binding protein (O'Rand et al., 1992) but has subsequently been shown to interact predominantly with H3 and H4 (Tagami et al., 2004; Campos and Reinberg, 2010; Cook et al., 2011). NASP displays multivalent interactions with its histone cargo: it binds with high affinity to a peptide epitope at the C-terminus of H3 via a canonical TPR-peptide interaction, and to an H3-H4 dimer via a secondary TPR surface site, possibly involving the acidic domain (Bowman et al., 2016, 2017). These differential interactions allow NASP to bind to H3 as both a monomer, and as an H3-H4 dimer in complex

with Anti-silencing factor 1 (ASF1) and other co-chaperones (Bowman et al., 2017; Apta-Smith et al., 2018; Groth et al., 2005; Alvarez et al., 2011; Campos and Reinberg, 2010). This is supported by the observation that NASP binds to a suprastoichiometric amount of H3 over H4, suggesting the existence of both an H3 monomer and an H3-H4 dimer pool *in vivo* (Apta-Smith et al., 2018). Further, such an encompassing role would agree with *in vivo* observations that NASP protects a soluble pool of H3-H4 against chaperone-mediated degradation (Cook et al., 2011).

Along with NASP, Retinoblastoma-Binding Protein-7 (RBBP7, formerly known as RbAp46 and closely related to it paralog RBBP4) together with Histone Acetyltransferase 1 (HAT1) form the HAT1-complex, which catalyses acetylation at lysines 5 and 12 on newly synthesised H4 (Verreault et al., 1998). HAT1 and RBBP7 can interact with H3–H4 together with ASF1 and NASP (Tagami et al., 2004; Ask et al., 2012; Groth et al., 2007), likely due to HAT1 and RBBP7 binding sites residing in the N-terminal tail (Wu et al., 2012) and first α-helix of H4 (Song et al., 2008; Murzina et al., 2008) away from the known binding sites of NASP and ASF1. However, whether HAT1-RBBP7 interact with a pool of monomeric H4, analogous to NASP and H3, has yet to be determined.

Using a combination of proteomics, in vitro binding, and pulse-chase analysis, we propose an import pathway and folding mechanism for monomeric H3 and H4 that specifically involves Imp5 binding and hand-off to nuclear chaperones NASP and HAT1-RBBP7, respectively. This pathway may represent a necessity to import histones faster than the kinetics of dimersation under periods of high need, such as during genome replication, working to alleviate potential bottlenecks in H3-H4 folding prior to nuclear translocation.

Results

Constitutively monomeric histones translocate to the nucleus

We recently suggested that, in addition to the canonical H3-H4 dimer import pathway, histone H3 and H4 can be imported into the nucleus in their monomeric state (Apta-Smith et al., 2018). To probe this further, we designed mutations in H3 and H4 that inhibit folding of the heterodimer. Two strategies were taken: breaking the $\alpha 2$ helix of the histone fold domain by insertion of three glycine residues (helix-breaker mutations, HB), and disruption of the histone fold by mutation of the hydrophobic core (fold-disruptor mutations, FD), (Fig. 1A and B). To validate their defective folding, histone mutants were expressed transiently in HEK293-F cells for 36 hours. Histone mutants were fused through a 22 amino acid linker to the N-terminus of eGFP for fluorescent detection, immunoprecipitation and western blotting (Fig. 1C and D). As expected, histone counterparts could be detected in wild-type pull-downs, but not in any of the non-folding mutants, even though the non-folding mutants were stable and expressed at comparable levels to wild type (Fig. 1C).

Interestingly, imaging of the eGFP-tagged histones revealed that all non-folding mutants were imported into the nucleus, however, they displayed a homogeneous fluorescent signal, indicative of a soluble, non-chromatin bound protein (Fig. 1D). Indeed, imaging of mitotic cells revealed wild-type histones locating to sister chromatids, whereas, the non-folding mutants were soluble (Fig. 1D). To further confirm the soluble nature of non-folding mutants we used Fluorescence Recovery After Photobleaching (FRAP). Whilst a photobleached area of nuclei expressing wild-type histones failed to recover over the duration of imaging, the non-folding mutants recovered fluorescence almost immediately (Fig. 1E). This suggest that eGFP-tagged wild-type histones are immobile, due to being incorporated into chromatin, whereas non-folding mutants are in rapid exchange with the bleached region, suggesting that they are not. In summary, these findings show that our designed non-folding mutants are not incorporated into chromatin, but do enter the histone chaperoning pathway in so far as they are imported into the nucleus and are not proteolytically degraded.

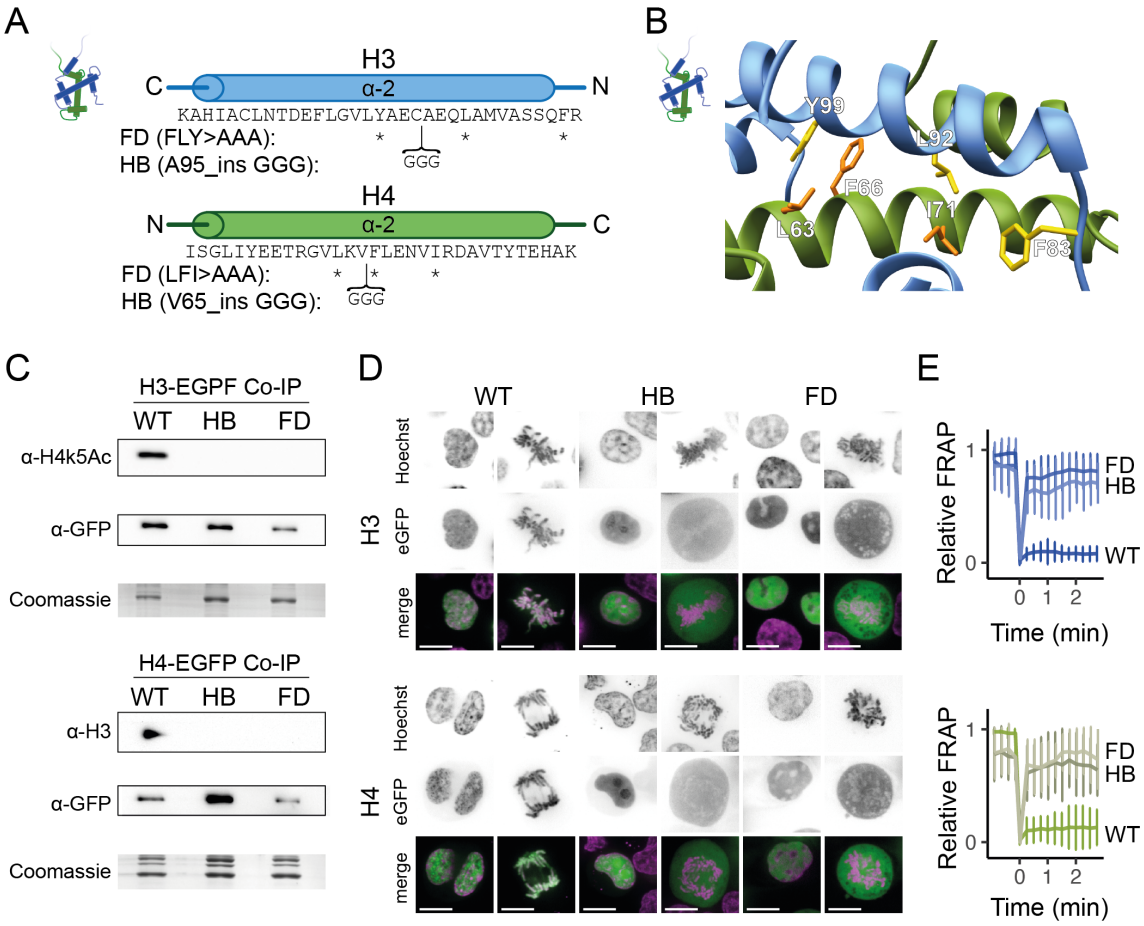

Figure 1: H3 and H4 dimerisation mutants translocate to the nucleus but do not incorporate into chromatin. **A**: Position of Fold-Disruptor (FD) substitutions (asterisks) and Helix-Breaker (HB) insertions (brackets). **B**: Positions of the fold-disruptor mutations superimposed on the H3-H4 heterodimer crystal structure (PDB: 2HUE). Residues targeted are shown in yellow for H3 and in orange for H4. **C**: Co-immunoprecipitation (Co-IP) analysis of the non-folding mutants confirms that they do not interact with their folding partner when expressed in HEK293-F cells as eGFP fusions, whilst their wild-type counterparts do. **D**: Confocal microscopy reveals non-folding mutants are imported into the nucleus, but do not localize to mitotic chromosomes. Scale bar indicates 10 µm. **E**: FRAP analysis of wild-type and mutant histones shown in D. Immediate recovery of fluorescence after bleaching confirms that the histone mutants are not chromatin-bound as are their their wild-type counterparts.

Non-folding histone mutants bind a specific subset of importins and chaperones

To identify factors that interact with histones in their monomeric state we performed co-IPs of the non-dimerising mutants followed by western-blotting (Fig. 2A). When probing known histone-binding factors, we found that both H3 and H4 lose their interaction with Imp4, but unexpectedly retain their interaction with the paralogue Imp5 (Fig. 2B). Interestingly, H3 mutants still interacted with NASP, but lost their interaction with HAT1 and RBBP7. Conversely, H4 mutants lost their interaction with NASP, but retained their interaction with HAT1 and RBBP7, whereas, both sets of mutants no longer interacted with ASF1A or B. (Fig. 2B).

We further investigated associating proteins using affinity-capture followed by mass spectrometry, confirming our findings by western blot (Fig. 2C) and allowing a non-biased analysis into unknown factors. By plotting normalised total precursor intensity of mutant against wild type, factors interacting equally with both histones were expected lie on the diagonal, with proteins interacting preferentially with wild type or mutants expected to reside above or below the diagonal, respectively (Fig. 2D).

Looking at histone H3, we found that histone chaperones previously characterised to interact with a constitutive H3-H4 dimer (ASF1A/B, CHAF1A/B, RBBP4, DNAJC9), the H4 tail-binding HAT1 complex (HAT1, RBBP7), Imp4 and histone H4 were enriched on wild-type H3 compared to mutants, as expected (Fig. 2A) (Groth et al., 2005; Tagami et al., 2004; Smith and Stillman, 1989; Tyler et al., 1999; Kleff et al., 1995; Hammond et al., 2021). Interactors that bound indiscriminately to wild type and monomeric H3 included the histone chaperones NASP, UBR7, C1QBP, Imp5, and to a lesser extent NAP1L1/4 and members of the HSP70 family of molecular chaperones HSPA1B, HSPA6 and HSPA8 (Fig. 2D). NASP has previously been demonstrated to interact with H3 both as a monomer and as an H3-H4 heterodimer (Bowman et al., 2016, 2017), whilst binding of the H3 tail region explains the non-selectivity of UBR7 (Kleiner et al., 2018). The interaction interface of the recently discovered chaperone C1QBP (Lin et al., 2021) has yet to be determined, however these findings suggest recognition of the H3-H4 dimer is not a prerequisite for binding. Interestingly, we found that Imp5 is highly enriched on both wild type and monomeric mutants, in stark contrast to its counterpart Imp4, which appears selectively enriched on the wild-type, in agreement with our western-blot analysis above (Fig. 2B).

Looking at histone H4, we found a similar pattern of binding with a few key differences. Whilst known H3-H4 binding proteins were selectively enriched with the wild-type histone, the HAT1 complex (HAT1 and RBBP7) bound indiscriminately to both wild-type and monomeric H4 (Fig. 2B). Conversely, NASP was present only with wild type but not monomeric mutants, again most likely reflecting an interaction interface orientated towards H3 (Bowman et al., 2016, 2017). Interestingly, UBR7 did not interact with either wild type or monomeric H4, suggesting that it may have specificity towards H3 in its monomeric state, potentially being displaced by H3-H4 dimer folding (Fig. 2D). This is in contrast to C1QBP, which associated with both wild type and monomeric mutants. Similar to H3, there was also discrepancy in the binding of importin proteins: whilst the wild type H4 enriched selectively for Imp4, Imp5 came down equally with mutant and wild type (Fig. 2B). These results suggest that Imp5 can interact with H3 and H4 in their monomeric state, whereas Imp4 is only able to interact with an H3-H4 dimer.

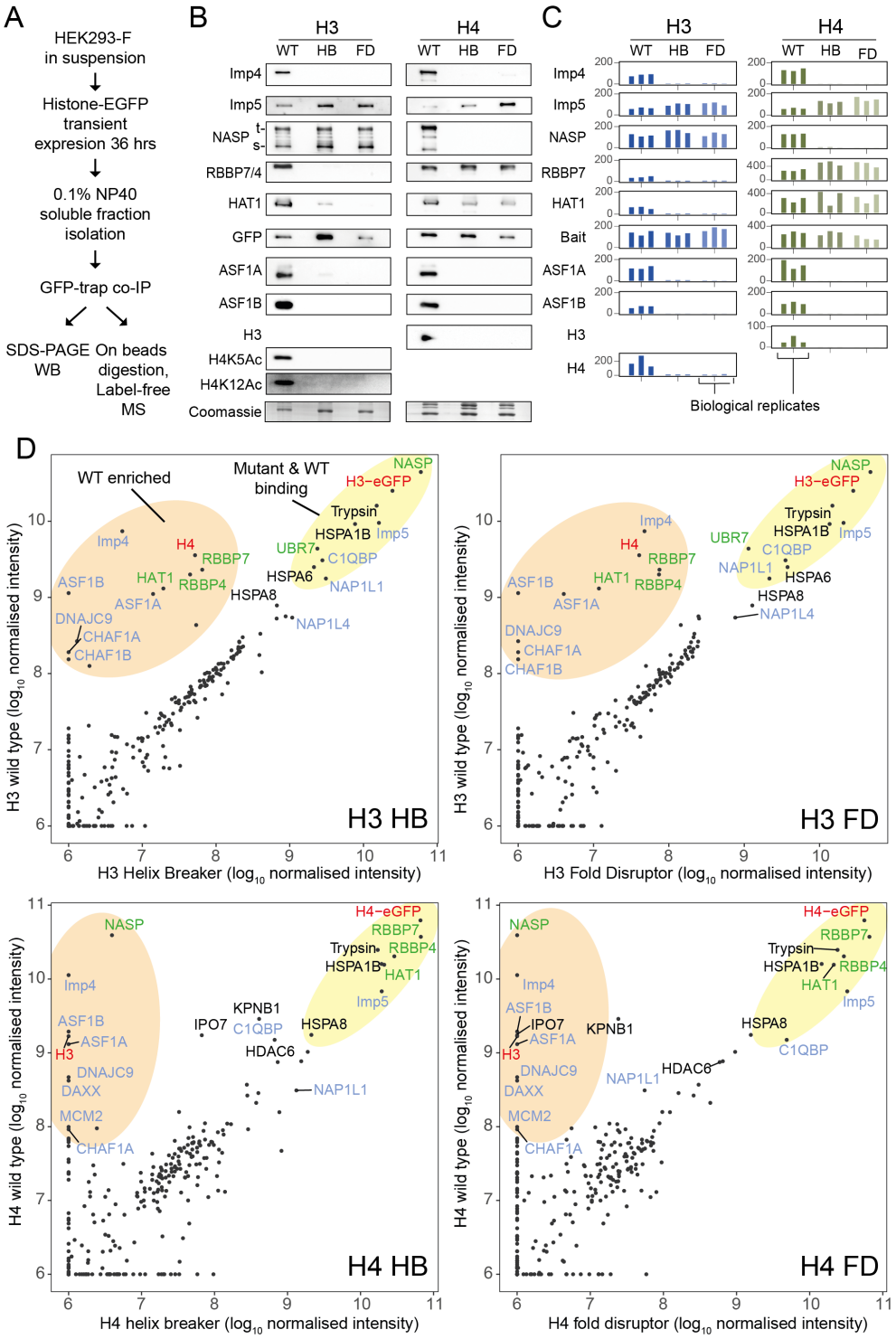

Figure 2: Monomeric histone interaction analysis. **A**: Experimental overview of histone expression and purification. **B**: Westernblot analysis of immunoprecipitated wild-type and monomeric histones probed for known histone interactors (HB, Helix Breaker mutation; FD, Fold Disruptor mutantion). **C**: Normalised total precursor intensity (10^6) of proteins of interest for H3 and mutants (blue) and H4 and mutants (green). Three biological replicates were performed. **D**: Proteomic anlaysis of wild type and monomeric histone mutants. The normalised total precursor intensity from three experiments are plotted as mutant against wild type. Circled regions show factors that are enriched for the wild-type (orange) or that are equally enriched on the wild type and mutant (yellow). Known histone-binding proteins are coloured in blue, with those that deferentially bind H3 and H4 mutants coloured in green. Histones are coloured in red.

NASP forms discrete H3 monomer and H3-H4 dimer containing complexes

To visualise the molecular interactions between the NASP TPR domain and the H3 C-terminal helix, we implemented the software AlpahFold2 (Deep Mind, London) (Jumper et al., 2021). In addition to predicting single protein folds, AlphaFold2 has also been shown to accurately predict protein interaction interfaces (Evans et al., 2021). Using ColabFold (AlphaFold2-Advanced) (Mirdita et al., 2021), we generated five predictions of the sNASP (residues 1-340) and the H3 C-terminal peptide (residues 116-135), of which all five were highly similar. Remarkably, AlphaFold2 positioned the H3 peptide within the putative peptide-binding groove of NASP. Furthermore, H3 residues that have previously been shown to be crucial for the interaction (Bowman et al., 2016) orientated towards the putative binding interface of the TPR domain (Fig.3A). Whilst not yet experimentally determined, this model lends support to the role of NASP as a H3 monomer binding chaperone.

To address whether endogenous NASP interacts with monomeric H3 under physiological conditions we generated CRISPR HeLa lines in which NASP and ASF1 loci were tagged with eGFP and mCherry, respectively (Fig. S2A and B), and performed one-step purifications using GFP/RFP Trap followed by quantification of H3:H4 ratios (Fig. 3B and C, Fig. S2C). In agreement with previous analysis of their over-expressed counterparts (Apta-Smith et al., 2018), as well as transient expression in HEK293-F cells, endogenously tagged NASP showed a 2.3-fold molar excess of H3 over H4, whereas ASF1 showed close to equimolar amounts of each. The excess H3 over H4 suggests the presence of multiple histone complexes, and that under physiological levels, NASP interacts with H3 in both its monomeric and H4-bound state.

To further interrogate NASP interactions we fractionated eGFP-sNASP pull-downs by 2D gel electrophoresis, the first dimension being native PAGE, and the second being SDS-PAGE, and probed them by western blotting. Separation by native PAGE yielded multiple sNASP containing bands, with separation of their constituents in the second dimension showing a clear H3 monomer containing complex and at least two H3-H4 containing complexes (Fig. 3D and E). Proteomic analysis of the native PAGE bands revealed three distinct histone-bound complexes: a sNASP-H3 monomer complex that also contained lower levels of UBR7, a sNASP-H3-H4-HAT1-RBBP4/7 complex, that has been well characterised previously (Campos et al., 2015; Campos and Reinberg, 2010; Alvarez et al., 2011; Tagami et al., 2004; Groth et al., 2005; Jasencakova et al., 2010), and a sNASP-H3-H4-RBBP4/7-ASF1 complex missing the HAT1 subunit of the HAT1 holocomplex (Fig. 3F).

In addition to these histone-containing complexes, a number of heat-shock proteins were also found associating with sNASP and so were the HDAC proteins 1 and 6 (Fig. S3), supporting previous findings (Campos et al., 2010; Alekseev et al., 2005; Apta-Smith et al., 2018). Strikingly, we did not detect Imp5 despite it co-purifying with monomeric histones (Fig.2D). Another interesting observation was the association of UBR7 with NASP and monomeric H3. UBR7 is a putative ubiquitin E3 ligase and has been previously identified to interact with histone H3 (Kleiner et al., 2018; Lambert et al., 2015; Campos et al., 2015; Foltz et al., 2009), but appears to be a novel interactor of NASP. Looking at the label free quantification, however, it is likely that UBR7-bound complex represents only a fraction of the total NASP-H3 present (roughly 10 percent), suggesting a secondary function to that of NASP-H3. In summary, NASP is found in three distinct complexes that are defined by their presence of monomeric H3 or heterodimeric H3-H4, but does not stably associate with Imp5.

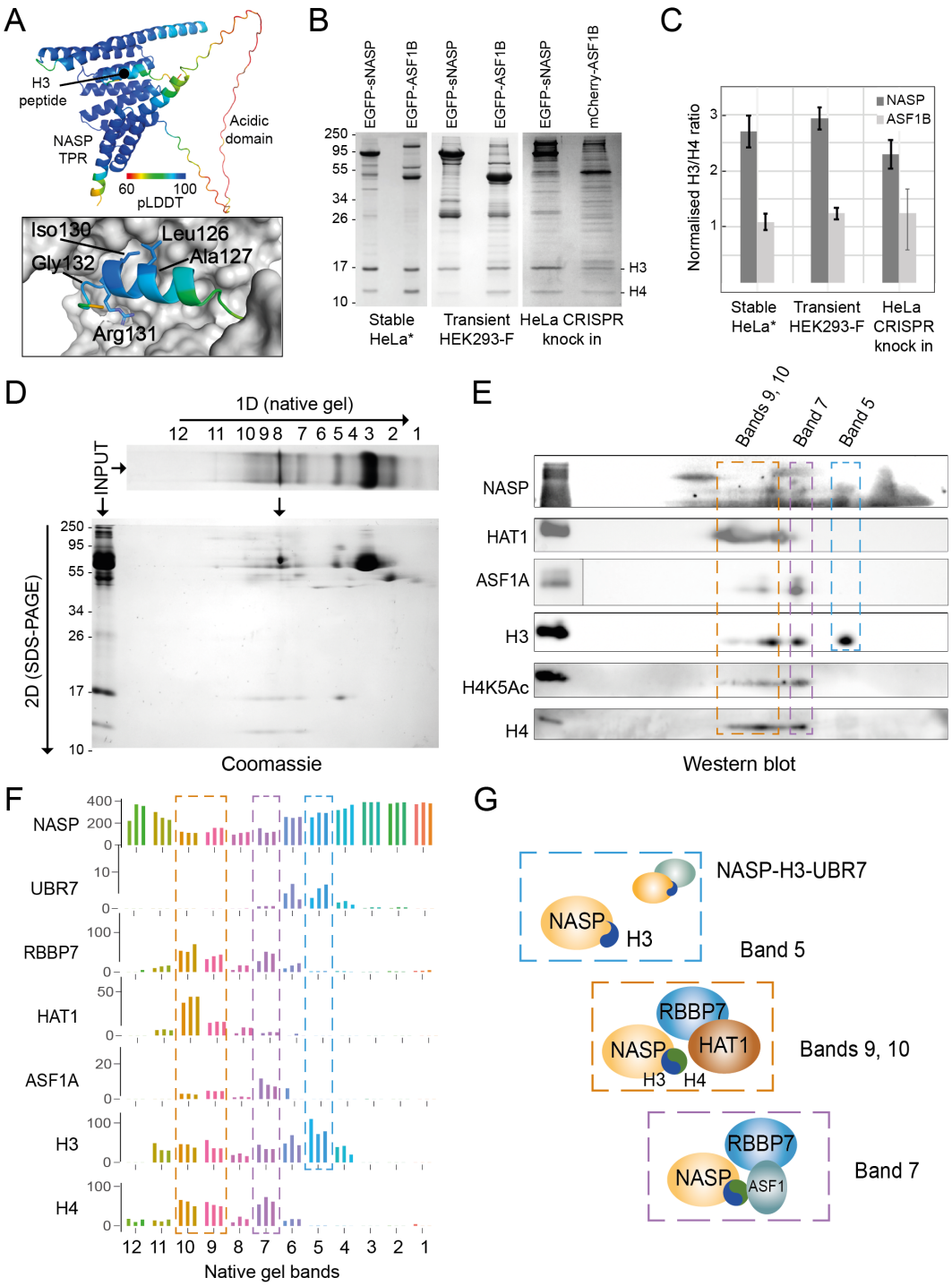

Figure 3: NASP associates with H3 and H3-H4 in discreet, multi-chaperone complexes. **A**: AlphaFold2 prediction of NASP-H3 peptide interaction coloured by per residue pLDDT scores (residues 1-30 of NASP omitted for clarity). Inset: detailed view of the H3 peptide binding prediction. Residues previously shown to be crucial for interaction are labelled and shown as sticks. H3 retains its pLDDT score colouring scheme. **B**: Histone chaperone immunoprecipitations separated by 15% SDS–PAGE and stained with Coomassie. Co-IPs for EGFP-NASP associated with NASP and ASF1 for stable HeLa cell lines, HEK293-F transient expression and CRISPR knock in engineered at their endogenous loci with eGFP and mCherry respectively. Asterisks mark previously published data (Apta-Smith et al., 2018). **C**: Ratios of H3 compared to H4 associated with NASP and ASF1 engineered at their endogenous loci with eGFP. Background-corrected densitometry profiles for the portions of the gels covering H3 and H4 were compared with gel filtration purified recombinant H3-H4 dimer. **D**: Native gel separation of immunoprecipitated eGFP-sNASP followed by SDS-PAGE to separate NASP-containing complexes. Band numbers correspond to gel sections that were analysed by mass spectrometry. **E**: Western blot analysis of 2D gel as shown in B. Blots were probed for known NASP-interacting factors. Note that a species containing H3 but not H4 is clearly discernible. **F**: Mass spectrometry identification of NASP-interacting factors from gel slices shown in D. **G**: NASP forms at least three distinct co-chaperone complexes: NASP-H3 /NASP-H3-UBR7, NASP-H3-H4-RBBP7-HAT1, NASP-H3-H4-RBBP7-ASF1.

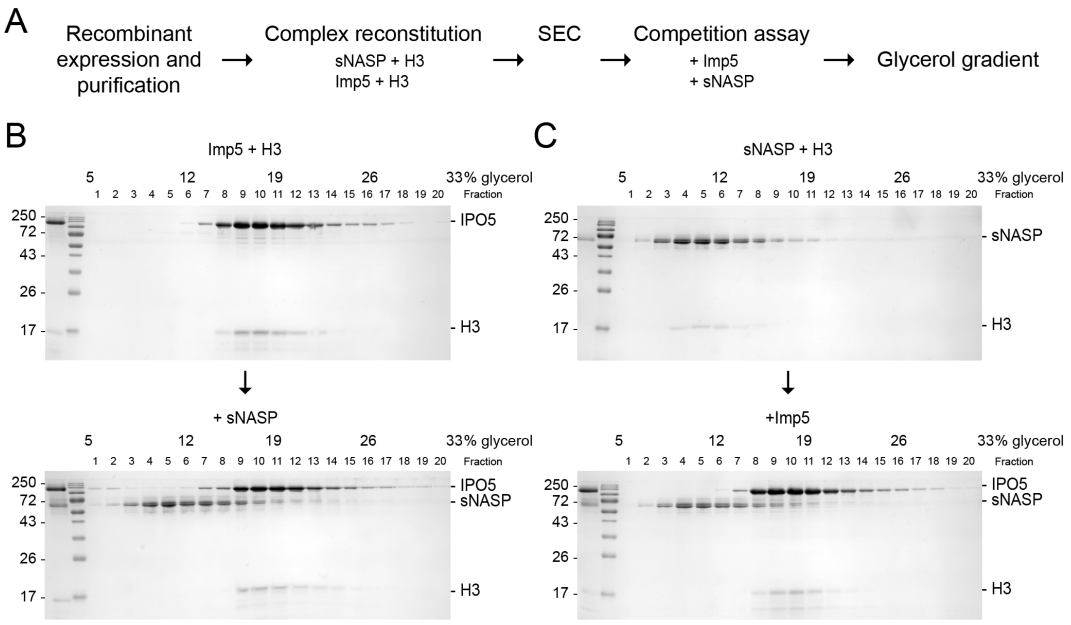

Figure 4: Imp5 and sNASP interaction with H3 is mutually exclusive. **A**: Experimental design. **B**: Imp5-H3 reconstituted complex was purified by SEC and incubated on ice (control, top) or with equimolar concentration of sNASP (competition assay) for 3 hours on ice before separating through ultracentrifugation on a 5-40% glycerol gradient. **C**: Conversely to C, sNASP-H3 reconstituted complex was purified by SEC and incubated on ice (control, top) or with equimolar concentration of Imp5 (competition assay) before separating through ultracentrifugation on a 5-40% glycerol gradient.

Mutual exclusivity between Imp5 and NASP in histone binding

Next, we asked whether binding of H3 by NASP and Imp5 is mutually exclusive or can occur concomitantly. To prevent extraneous factors affecting our analysis, we used purified recombinant proteins reconstituted *in vitro* (Fig. 4A). Imp5 was able to bind equimolar concentrations of histone H3 and histone H4 when separated by size exclusion chromatography, demonstrating a direct interaction with histones (Fig. S4A). However, size exclusion chromatography was unable to resolve sNASP and Imp5 elution profiles sufficiently to allow unambiguous assignment(Fig. S4B). However, they were found to separate well by ultracentrifugation on a glycerol gradient, suggesting that in the absence of histone cargo sNASP and Imp5 do not interact directly (Fig. S4C).

Purified Imp5-H3 complex was combined with an equimolar amount of sNASP and left to equilibrate for three hours on ice before separation. Interestingly, Imp5-H3 and sNASP eluted in separate fractions, suggesting that sNASP cannot bind to H3 whilst it is in complex with Imp5, and that sNASP does not compete with Imp5 for histone binding under these experimental conditions (Fig. 4B). Remarkably, when the reverse experiment was performed, Imp5 was able to strip sNASP of its histone, with almost all of the H3 co-fractionating with the importin rather than NASP (Fig. 4C). This suggests that, firstly, as pre-assembled complex was used as input, NASP-H3 has a dissociation rate significantly below the incubation time for competition (three hours), secondly, Imp5 has a significantly higher dissociation constant than NASP towards monomeric H3, and thirdly, the dissociation of Imp5-H3 *in vivo* likely requires additional factors, such as release by RanGTP. In summary, direct binding competition towards H3 likely represents the absence of complex formation between IPO5 and NASP, even though both proteins interact with H3 in its monomeric state *in vivo*.

H3 associates with Imp5 in the cytoplasm transferring rapidly to NASP in the nucleus

We recently developed the pulse-chase method 'RAPID-release' enabling biochemical and microscopy observations of histone nuclear translocation. The system consists of two components: the histone cargo with a cytoplasmic tether localising to the outer mitochondrial membrane, and a protease that

can be locally activated through rapamycin-induced recruitment (Apta-Smith et al., 2018). The system is highly adaptable and can be modified to study both localisation and interactions using appropriate functional tags (Fig. 5A).

Initially we employed a non-bias approach using proximity biotinylation via the APEX tag (Lam et al., 2015) in a doxycycline-inducible FRT HeLa cell line. However, H3-APEX-EGFP-RR presented slower release kinetics when compared to the original RAPID-release, possibly due to the increase in steric hindrance derived from a considerably longer fusion construct (Fig. S5B). Due to this we chose two time points: an initial time point representing the cytoplasmic state (0 min) and a time point sufficient to ensure near-complete nuclear translocation (120 min). To control for unspecific interactions, we contrasted our results with a control comprised only of APEX2 tethered to the outer mitochondrial membrane.

Interestingly, Imp4 and Imp5 are over 100-fold enriched on cytoplasmically-tethered histones (0 min) compared to released histones (120 min). Similarly, we do not observe NASP, ASF1B, the MCM2-7 complex or RBBP4 in the proximity of cytoplasmic histones, but do observe them interacting once histones that have been released and reached to the nucleus (Fig. 5C and D), supporting our previous findings that these chaperones interact with histones overwhelmingly in the nucleus and not in the cytoplasm of the cell (Apta-Smith et al., 2018).

To investigate the Imp5-H3 cytoplasmic interaction, we next co-transfected HeLa cells with Imp5-eGFP and H3-mCherry-RAPID-release and found that Imp5 is enriched on mitochondrially tethered H3 (Fig.5D), similar to what has previously been seen using Imp4 (Apta-Smith et al., 2018). Additionally, this colocalisation disappeared when rapamycin was added to the cells, with H3 being imported rapidly and Imp5 remaining in the cytoplasm (Fig5E), suggesting that the Imp5-H3 interaction is specific, and that hand-off to the nuclear chaperoning machinery is a rapid event.

Similarly, using the CRISPR engineered EGFP-NASP cell line (Fig. 3B), we introduced H3-mCherry-RR and studied NASP association with newly synthesised histone H3. Endogenously expressed EGFP-NASP was entirely nuclear, with no enrichment over the tethered histone (Fig. 5F). Release of H3-mCherry by addition of rapamycin followed similar kinetics to previously described H3-EGFP (Apta-Smith et al., 2018), resulting in a half maximum cleavage at around 10 min (Fig. 5G). Unlike Imp5, association could not be inferred from the microscopy alone, so we performed Co-IPs at 10 min, 1 hour and 24 hour intervals after histone release(Fig. 5H). Interestingly, H3's association with NASP peaked at the 10 minute time point, when the nucleus experiences the highest surge of the released histone, strongly suggesting that NASP associates with H3 as it enters the nucleus. Association with H3 was also present at later time points, with 24 hours likely to represent an equilibrium between soluble and chromatin-bound state. This would suggest that NASP can also interact with post-nucleosomal histone, and is not necessarily limited to the interaction with incoming, newly synthesised H3. Taken together, these findings allude to NASP being the predominant nuclear receptor for monomeric H3 via rapid hand off event from Imp5.

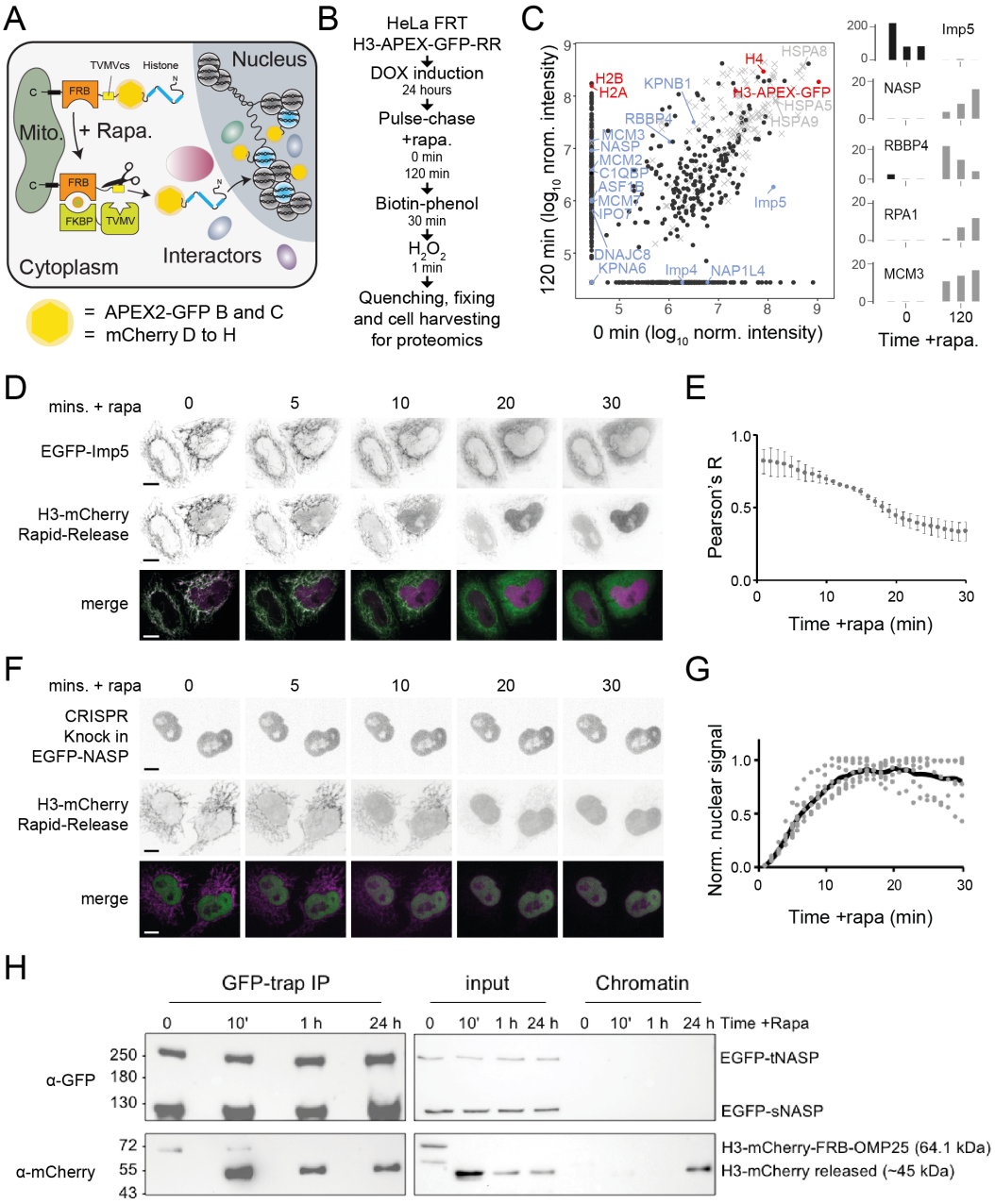

Figure 5: H3 binds Imp5 in the cytoplasm and transfers rapidly to NASP upon nuclear import
A: Experimental design combining a histone pulse with co-immunoprecipitation. Addition of rapamycin recruits an otherwise auto-inhibited TVMV protease which cleaves the tethered histone fusion allowing it to enter the histone deposition pathway. **B**: Experimental design for doxycycline-inducible H3-APEX2-EGFP-RAPID-Release (H3-APEX2-EGFP-RR). **C**: Left, normalised total precursor intensity of proteins detected by label-free mass spectrometry after sptreptavidin pull-down (as described in A and B). Histones are coloured in red, known interaction factors in blue and proteins detected in the control experiments in gray 'x'. Right, representation of the normalise total precursor intensity of known histone interacting factors. **D and E**: EGFP-Imp5 and H3-mCherry-RR transient expression co-localization and Pearson's correlation coefficient before and after exposure to rapamycin (+rapa). Scale bar indicates 10 µm. **F and G**: EGFP-NASP endogenously labelled by CRISPR knock-in and H3-mCherry-RR stable expression co-localization and nuclear enrichment analysis before and after exposure to rapamycin (+rapa). Scale bar indicates 10 µm. **H**: Westernblot analysis of anti-GFP co-immunoprecipitated proteins (Co-IP) from EGFP-NASP endogenously labelled by CRISPR knock-in and H3-mCherry-RR stable expression HeLa cell line.

Discussion

Here we propose a novel nuclear import pathway governing the transfer of monomeric H3 and H4 from Imp5 to histone-specific nuclear chaperones. Although both Imp4 and Imp5 have H3-H4 binding capacity, it is only Imp5 that can also interact with monomeric versions of the histones. Whilst Imp4 has long been shown in pulldowns with H3-H4 (Groth et al., 2005; Tagami et al., 2004; Campos and Reinberg, 2010; Yoon et al., 2018; Mosammaparast et al., 2002, 2001), the mode of selectivity towards a dimeric cargo is not yet clear as Imp4 interaction studies have predominantly focused on interactions with the histone N-terminal tail regions (Yoon et al., 2018; Mosammaparast et al., 2002, 2001). Our forced monomeric mutations do not reside within this region of H3 or H4, yet we do not see Imp4 associating with them, eluding to a more intricate association than a simple importin-histone NLS binding mechanism.

Conversely, we show that Imp5 associates strongly with monomeric H3, both *in vivo* and *in vitro*, and that binding is mutually exclusive with NASP (Fig. 4). This was unexpected as NASP interacts predominantly with the C-terminal region of H3 (Bowman et al., 2016), outside of the previously characterised N-terminal importin-binding region. In addition, we show here that Imp5 can outcompete NASP for H3 *in vitro*, which has high affinity towards its histone cargo (Bowman et al., 2016), suggesting that Imp5 makes extensive interactions with H3 outside of the characterised H3 tail region (Soniat et al., 2016). Whilst structural characterisation of full-length histones in complex with importin proteins is necessary to fully understand these hand-off events, it is intriguing that Importin-9 encapsulates a whole H2A-H2B dimer within its HEAT repeats, making significant interactions with the histone fold domain, rather than the N-terminal tail regions (Padavannil et al., 2019). A related mode of interaction could be consistent with our characterisation of Imp5-H3-NASP binding behaviour.

The rapid association of newly synthesised H3 with NASP suggests that NASP acts as a nuclear receptor accepting H3 from Imp5 (Fig. 5). The necessity to sequester a monomeric histone may relate to the folding kinetics of H3-H4 relative to nuclear import. NASP may therefore be regarded as having a 'holdase' function, as has been suggested for the ATP-independent small heat shock protein family of molecular chaperones (Jakob et al., 1993; Mymrikov et al., 2017; Ecroyd, 2015; Taipale et al., 2014; Mogk and Bukau, 2017; Reinle et al., 2021). In addition, the presence of NASP in downstream complexes, mediated by interactions outside of the TPR-H3 peptide interface (Bowman et al., 2017), further supports NASP having a role in guiding the transition from monomeric import to a heterodimer capable of DNA deposition.

Unexpectedly, we found the ubiquitin ligase UBR7 in the same native fraction as NASP and H3 (Fig. 3). UBR7 has been previously implicated with chromatin processes. UBR7 associates with H3, and its centromeric homolog CENP-A, (Campos et al., 2015; Foltz et al., 2009; Lambert et al., 2015; Kleiner et al., 2018), with proposed interactions occurring between its PHD finger domain and the methylated tail of H3 (Kleiner et al., 2018). Additionally, UBR7 is also responsible for H2BK120 directed monoubiquitin ligase activity (Adhikary et al., 2019). The function of UBR7 in the context of soluble H3 is less clear, and need not relate directly to the major function of the NASP-H3, with quantification suggesting it was roughly ten percent of the NASP-H3 pool. Similarly, we detect the new chaperone C1QBP (Lin et al., 2021) bound to monomeric mutants of both H3 and H4 at similar levels to UBR7. However, we do not see association with NASP, suggesting a potential upstream function. The role of these new proteins in the histone chaperoning pathway will require further analysis to reveal their true functions.

As a counterpart to NASP-H3, the holoenzyme HAT1-RBBP7 interacts with both monomeric histone H4 mutants, suggesting that HAT1-RBBP7 may accept monomeric histones from Imp5 in the nucleus. However, in our previous analysis, we could not isolate the amounts of H3 or H4 bound to HAT1 for quantification of H3:H4 ratios (Apta-Smith et al., 2018). Thus, we have not been able to ascertain whether HAT-RBBP7 interacts with a pool of monomeric H4 in the nucleus, analogous to NASP's interaction with H3. Structural characterisation of the homologous Hat1p-Hat2p complex from yeast, suggests that dimerisation with H3 is not necessary for interaction with H4, which is me-

diated predominantly with the H4 tail and α1 region (Li et al., 2014). The HAT1-RBBP7 complex is responsible for lysine K5 and K12 acetylation in newly synthesied histone H4 (Verreault et al., 1998). Interestingly, in native isolation of NASP-associated complexes, we find histone H4 K5 acetylation peaking in bands that lack any significant HAT1 enzyme (Fig. 3), suggesting a temporal transition from an earlier sub-complex of NASP-RBBP7-HAT1 where the catalytic activity may take place. The low levels of ASF1 detected in this complex is notable, and may elude to transitory state in which the TPR domain of NASP is still engaged with the C-terminal region of H3 which is necessary for ASF1 binding to H3-H4 (English et al., 2005; Natsume et al., 2007).

In summary, we propose a monomeric histone supply pathway for H3 and H4 fed by the importin Imp5 that transfers histones to NASP and HAT1-RBBP7, respectively. In this model, NASP and HAT1-RBBP7 provide a holdase function for monomeric histones that smooths imbalances in histone production, negates the requirement for cytoplasmic folding and provides a kinetic pathway for the assembly of the H3-H4 heterodimer.

Materials and Methods

Cloning and plasmid material

Plasmids were constructed through a mixture of PCR cloning, annealed oligo ligation, gBLOCK synthesis (IDT™) and Gibson assembly (Gibson, 2009). All constructs were sequence-verified by Sanger sequencing. Plasmids can be found in Table S1. Primer sequence and DNA fragments are in Table S2.

The open reading frame from Imp5 isoform 1 (Uniprot identifier: O00410-1) was amplified from HeLa cDNA and ligated into pEGFP-C1 with XhoI and KpnI sites (EGFP-Imp5). For bacterial protein expression Imp5, was re-cloned and digested with BamHI and NotI and ligated into pGEX-6P1 (Cytiva) cut with the same enzymes. $(His)_6$-sNASP, H3 and H4 histones constructs have been detailed previously (Bowman et al., 2016, 2017).

The RAPID-release plasmids were used as previously published (Apta-Smith et al., 2018). In order to contain the 2-component RAPID-release system in a single vector the tethered cassette (H3.2mCherry-TVMVcsx2-FRB-OMP25) and the protease cassette (FKBP12-TVMV-AI) were cloned either side of an Internal Ribosome Entry Site (IRES) in the vector pEGFP-IRES-Puro (Addgene #45567) replacing the EGFP and Puro cassettes with the RR components to from pH3.1-mCherry-RR.

CRISPR knock-in cell lines were obtained following the D10ACas9 nickase using the paired guide RNAs protocol (Ran et al., 2013). For the Homologous DNA Repair (HDR) template, 800 bp upstream and downstream of the start codon from exon 1 of NASP and ASF1B were amplified from genomic DNA, and ligated through Gibson assembly to EGFP and mCherry, respectively, so that an in-frame 5' fusion to exon 1 was formed. This was cloned into pBlueScript II KS (+) as destination plasmid. Guide RNAs were prepared as described, combining two complementary oligonucleotides with CACC / AAAC overhangs into D10ACas9 vector pX461-PSPCas9N(BB)-2A-GFP (Addgene #48140) cut with BbsI.

For the inducible expression of H3-APEX-GFP-RR, the H3.1-APEX2-EGFP-2xTVMVcs-FRB-OMP25 –IRES– FKBP12-TVMV-AI (pH3-APEX2-EGFP-RR) construct was inserted through Gibson assembly, using synthetic DNA fragment for APEX2 DNA sequence (IDT), into pcDNA™FRT/TO (Thermo) plasmid for recombination in the HeLa Flp-In™ T-REx™ system. See plasmid sequences in Table S1 and primer sequences and DNA fragments in Table S2 for details.

Protein expression and purification

All recombinant proteins were produced in Rosetta *Escherichia coli* competent cells induced with 0.4 mM isopropyl-β-d-1-thiogalactoside (IPTG) at an OD_{600} of 0.6, unless otherwise stated. sNASP was expressed overnight at 21 °C as an N-terminal $(His)_6$ fusion construct and purified using Ni-NTA affinity resin (Cytiva) and further purified by ion-exchange chromatography after cleavage of the $(His)_6$ fusion by TEV protease as previously described (Bowman et al., 2016).

Importin-5 (Imp5) purification was addapted from Soniat et al. (2016). GST-Imp5 construct was induced for 12 hours at 24 °C. Bacteria were pelleted and lysed in 50 mM Tris, pH 7.5, 150 mM sodium chloride, 20% glycerol, 2 mM dithiothreitol, 1 mM EDTA, protease inhibitors and lytic cocktail (10 µg/mL RNase A, 100 µg/mL DNase I, 1 mg/mL Lysozyme) for 2 hours at 4 °C, followed by flash-freezing in liquid nitrogen. Pellets were rapidly thawed at 37 °C and quickly placed on ice before sonication with a Misonix sonicator (3 pulses 'on' for 10 seconds and 'off' 30 seconds with an amplitude of 25). Imp5 was then purified with GST-trap resin (Cytiva) and further purified by anion-exchange chromatography following overnight cleavage by 3C protease.

Full length *Xenopus laevis* histones H3 and H4 were purified and refolded as previously described (Luger et al., 1997).

Analytical gel filtration

Analytical gel filtration was carried out using a Superdex Increase 200 10/300 column (GE Healthcare) in 20 mM HEPES-KOH pH 7.5 and 150 mM sodium chloride, unless otherwise stated. 0.6 ml fractions were collected encompassing the void and bed volumes of the column. Proteins and complexes were reconstituted at a concentration of 20 µM. Fractions were separated by SDS-PAGE and stained with Coomassie Brilliant Blue (Instant Blue®, Abcam).

Competition assay and glycerol gradient ultracentrifugation

Purified Imp5 or sNASP were mixed with equimolar amount of histone H3 (20 µM final concentration) in 20 mM HEPES-KOH pH 7.5, 150 mM sodium chloride, 2 mM magnesium acetate, 1 mM EGTA, 2 mM dithiothreitol and 10% glycerol and allow to equilibrate for 10 min on ice before spinning at 20,000 g for 20 min at 4 °C to remove any precipitate. The sample was loaded for size exclusion chromatography on Superdex Increase S200 10/300 column (GE Healthcare) and central fractions were pooled, concentrated with a 10 kDa concentrator and quantified.

For glycerol gradient ultracentrifugation, preformed Imp-H3 and sNASP-H3 complexes were combined with an equimolar amount of sNASP or Imp5, respectively, and left to equilibrate for three hours on ice before separation (adapted from (McClelland and McAinsh, 2009)). Briefly, protein mixtures were diluted (at least 5-fold) to 6.25 µM or 1250 pmoles of protein in 200 µL of gradient loading buffer (20 mM HEPES pH 7.5, 150 mM sodium chloride, 2 mM dithiothreitol, 1% glycerol) and gently layered on a 5 mL gradient of 5–40% glycerol (20 mM HEPES pH 7.5, 150 mM sodium chloride, 2 mM dithiothreitol) made with Gradient Master (BioComp): Program Short Glycerol 5-40%. The samples were spun on a pre-chilled Optima XPN-80L ultracentrifuge (Beckman Coulter), rotor Sw55Ti, at 240,000 g for 14 hours at 4 °C. 200 µL fractions were manually collected, mixed 4:1 with 4xSDS sample buffer, boiled for 5 min and loaded on 15% SDS-PAGE for Coomassie staining (Instant Blue®, Abcam).

Tissue culture and cell lines

HeLa Kyoto cells (originally sourced from CRUK Cell Services, and cultured in house) were grown to 70% confluency in DMEM-Hi glucose (Gibco) supplemented with 10% heat-inactivated foetal bovine serum (Sigma), 50 µg/ml penicillin/streptomycin at 37°C in a humidified incubator with 5% CO_2. Cells were passaged with 0.25% trypsin-EDTA and resuspended in complete media. Cells were transfected following the Fugene® HD manufacturer's instructions (Promega). The day before transfection, cells were passaged, counted and plated at appropriate cell density ($2.5x10^5$ or $2.5x10^4$ cells per well for a 6-well plate and an 8-well µ-slides (ibidi), respectively). Transfection mixtures contained 1 µg plasmid DNA per 3 µL Fugene HD transfection reagent in 50 µL PBS. The transfection mixture was incubated at room temperature for 10 min prior to addition to cells. Cells were transfected with 12.5 µL or 100 µL of the transfection mixture per well for an 8-well µ-slide or 6-well plate, respectively. Cells were imaged 24-48 hours post-transfection.

To generate stable lines, HeLa or HeLa FRT cells were transfected as described above in 6-well plate when 70% confluent. After 48 hours, the media was changed with media containing selection antibiotic and split when required. 14 days after transfection, cells were sorted into fluorescent-positive single cells through FACS.

HEK293-F cells were grown in suspension to $1x10^6$ cells/mL with serum-free FreeStyle 293 expression medium (Thermo Fisher), supplemented with 25 µg/ml penicillin/streptomycin, in a humidified incubator with 8% CO_2 and 120 rpm. HEK293-F cells were split 24 hours before transfection to $0.5x10^6$ cells/mL, and transfected with 1 µg of DNA per $2x10^6$ cells and 3 µg of linear PEI per 1 µg of DNA in OptiMEM (60 µL per 1 µg of DNA), vortexed briefly and incubated at room temperature for 15 min before adding to the cells.

CRISPR knock-in cell lines

HeLa CRISPR knock-in cell lines were obtained following the established protocol (Ran et al., 2013). Briefly, cells were co-transfected with plasmids encoding upstream and downstream sgRNA, the D10ACas9 nickase and a homology directed repair template on 6-well plates at 70% confluency using FuGene® HD (Promega). Cells were allowed to recover for 7-10 days (splitting if necessary) before single clone selection through flow cytometry.

Flow cytometry

Single HeLa and HeLa FRT cells were sorted with a BD FACSAria™ Fusion Flow Cytometer, using a 100 µm nozzle, gating FSC-A/FSC-H for singlets and laser compensation using negative and positive controls. Cells were harvested by incubation with trypsin-EDTA for 5 min as before, and rinsed in PBS twice by centrifugation at 200 g for 5 min at 4 °C. Then cells were resuspended in phenol red-free DMEM supplemented with 2% FBS, filtered through a 50 µm Cell Strainer cap (Falcon) and maintained on ice until flow cytometry. Cells were sorted into 96 well plates with 1000 µL 1:1 fresh DMEM:conditioned DMEM (from pre-sorted medium) and 20% FBS.

Cell fractionation

Cell fractionation was performed following the REAP protocol (Suzuki et al., 2010) as previously adapted by Apta-Smith et al. (2018). Either cells on plates or cells on suspension were washed twice with PBS before collection. Cells on suspension were pelleted at 200 g, 5 min, 4 °C between washes. Adherent cells were scraped into 1 ml ice-cold PBS and pelleted the same way before resuspension in lysis buffer (0.1% NP-40 in PBS containing the protease inhibitors PMSF, aprotinin, leupeptin, pepstatin and benzamidine).

Lysis was continued for 10 min on ice, before pelleting of the chromatin fraction for 10 min at 1,000 g 4 °C. The supernatant was again spun at 2,000 g 4°C, and then removed to a fresh tube and spun for 20 min at 20,000 g to remove any membrane debris. For Co-IP experiments, in order to ensure identical loading across samples, the amount of GFP-bound protein was assessed by running 6 µL of final extract with 2 µL 4xSDS sample buffer (without boiling) on a Mini-PROTEAN TGX Precast Gel (BioRad), visualised with LED_{488} illumination (G-box, Syngene) and quantified against recombinant GST-EGFP using ImageJ software (Fig.S1).

Immunoprecipitation

Soluble cell fractions were bound to 10 µL per mL of lysate of GFP-Trap® (ChromoTek™) agarose beads. Binding was allowed to proceed for 1 hour at 4°C with continual nutation. Beads were spun for 2 min at 250 g, 4 °C and washed once in 20 mM Tris–HCl pH 7.5, 400 mM sodium chloride and 0.1% NP-40 (high salt buffer), followed by three washes in PBS + 0.1% NP-40, and one last wash in PBS. For SDS-PAGE analysis, the beads were either boiled directly in 40 µL 2xLaemmli sample buffer. For 1D Native PAGE, the beads were incubated in PBS 2 µM dithiothreitol, at 4 °C for 16 hours with TEV protease to release bait complexes. For mass spectrometery, the beads were washed four times with 50 mM ammonium bicarbonate, alkylated in 10 mM TCEP, 40 mM CAA in 50 mM ABC for 5 min at 70 °C and incubated with 1 µg Trypsin per 100µg protein and digested at 37 °C overnight.

Native gel (1D) and 2D gel separation

After overnight TEV cleavage, soluble samples were separated from GFP-trap matrix by filtration through 0.22 µm nilon filter (Co-star) spun at 2,000 g for 2 min at 4 °C. Protein complexes were concentrated to 25 µL in 30 kDa centrifugal concentrator (Vivaspin 500 Sartorius) and mixed with equal volume of 2 x native gel sample buffer: 62.5 mM Tris-HCl, pH 6.8, 40% glycerol, 0.01% bromophenol blue (BioRad). Three lanes were loaded with 15 µL each on a 4-20% polyacrylamide Mini-PROTEAN TGX Precast Gel (BioRad) and run with 25 mM Tris, 192 mM glycine, pH 8.4 buffer. The gel was run for 6 hours below 10 mA (20 min at 20 V, 30 min at 30 V, 60 min at 60 V, 120 min at 120 V

and 120 min at 160 V). The gel lanes were longitudinally cropped, using one of them for Coomassie staining, from which bands were cut and stored at -80 °C until mass-spectrometry analysis. Gel bands were in-gel digested according to (Shevchenko et al., 2006). The other two lanes were incubated with 1xTris/glycine/SDS buffer for 15 min and then incubated with 2 x Laemmli sample buffer (BioRad) for 15 min, heated twice for 15 seconds in the microwave (800 mA) and loaded on 15% polyacrylamide gel for 2D separation. One gel was dedicated to Coomassie staining and the other one was used for western blot analysis.

Coomassie stain and western blot analysis

Pellets of nuclear fractions were resuspended in lysis buffer with 1 µL benzonase (Sigma). The cytosolic fractions were diluted in Laemmli sample buffer and boiled for 5 min. Samples were run on 15% acrylamide gels for separation of histones H3 and H4. Coomassie staining was performed with InstantBlue (Abcam), following manufacturer's instructions. Gels for western blots were transferred using iBlot 2 Dry Blotting System (Thermo Fisher) onto a nitrocellulose membrane, blocked with 3% powdered milk in TBS-T and then incubated at 4°C overnight with primary antibodies diluted in 3% powdered milk or 3% BSA. Antibody dilutions were made at 1:1,000 ratios except anti-NASP (Apta-Smith et al., 2018), which was diluted to 1:10,000-40,000). Membranes were washed with TBS-T and then incubated for 1 h at room temperature with the HRP-conjugated secondary antibody. See Table S3 for list of antibodies.

APEX biotinylation and sample preparation

Proximity biotinylation was performed according to (Lambert et al., 2015). Briefly, per condition, four 15 cm^s plates were induced for 24 hours with 0.5 µg/mL doxycycline for the expression of H3-APEX2-EGFP-RR. Rapamycin (200 nM final) was added 120 min before harvesting to release histone H3-APEX2-EGFP, compared to mock-treated cells (time 0). Thirty minutes before harvesting, cell media was supplemented with biotin-phenol (Iris Biotech) to final concentration of 500 µM and incubated for 30 min at 37 °C 5% CO_2, before 200 µL per 15 cm plate of 100 mM H_2O_2 (final concentration 1 mM) was added and incubated for 1 min at room temperature with gentle shaking (100 mM stock was prepared from fresh H_2O_2 Merck 30% w/w). The reaction was quenched by washing cells three times with ice-cold 5 mM trolox, 10 mM sodium ascorbate, 0.03% sodium azide in PBS. Cells were scraped off the plates and lysed with RIPA lysis buffer (50 mM Tris-HCl, pH 7.5, 150 mM sodium chloride, 0.1% SDS, 0.5% sodium deoxycholate, 1% Triton X-100, protease inhibitors (as detailed above) and 2 µL benzonase (Sigma)) for 20 min on ice. Lysates were clarified by centrifugation at 16,000 g for 10 minutes at 4 °C before protein concentration was determined by Bradford assay. 25 µL of Pierce™ High Capacity Streptavidin Agarose (Thermo Fisher) was used for each condition. Lysates of equal protein concentrations were incubated with streptavidin beads for 60 min at 4 °C , washed twice with cold lysis buffer, once with cold 1 M KCl, once with cold 100 mM sodium carbonate, once with cold 2 M urea in 50 mM ammonium bicarbonate and three times in 50 mM ammonium bicarbonate. Samples were alkylated in 10 mM TCEP, 40 mM chloroacetamide in 50 mM ammonium for 5 min at 70 °C and digested with 1 µg trypsin per 100µg protein 37 °C overnight. The pH was adjusted to 3.5 before peptide storage at -20 °C for MS.

LC-MS/MS and data analysis

Peptides from on-gel digestion or on-beads digestion were analysed on a Orbitrap Fusion with UltiMate 3000 RSLCnano System (Thermo Scientific). The raw data were searched using MaxQuant software (Version: 1.6.10.43) against UniProtKB Human database and the common contaminants database from MaxQuant (Tyanova et al., 2016) from peptides generated from a tryptic digestion.

The software Scaffold (TM, Version: 4.8.9, Proteome Software Inc.) was used to validate MS/MS-based peptide and protein identifications. With the exception of BioID experiments, peptide identifications were accepted if they could be established at 95% probability or higher by the Scaffold Local FDR algorithm. Protein identifications were accepted if they could be established at 99% probability

or higher and contained at least two identified peptides. For BioID experiments thresholds were 95% for peptide identification, 95% for protein identification containing at least two peptides. Proteins that contained similar peptides and could not be differentiated based on MS/MS analysis alone were grouped to satisfy the principles of parsimony. Proteins sharing significant peptide evidence were grouped into clusters.

Imaging

All images were captured using an UltraVIEW VoX Live Cell Imaging System (PerkinElmer) with a 37°C environmental chamber. Live cell imaging involved culturing cells in 8-well µ-slides (ibidi) and replacing medium with 200 µL Leibovitz's L-15 (L-15) medium (Thermo Fisher Scientific) supplemented with 4 mM l-glutamine and 50 µg/ml penicillin/streptomycin. If indicated, cells were stained with 1 µg/ml Hoechst for 10 min and washed with PBS before addition of L-15 medium.

For RAPID-release experiments, Leibovitz's medium containing 1 µM rapamycin was added directly to the well resulting in a final concentration of 200 nM rapamycin. An initial image stack was taken prior to rapamycin addition, serving as time 0, after which cells were imaged every minute for up to 30 min.For RAPID-release of tethered H3.1-mCherry and soluble EGFP-Imp5, cells were co-transfected with H3.1-mCherry-RR and EGFP-Imp5 with release being performed as described above, allowing H3.1 and Imp5 to be followed in the red and green channels, respectively. For RAPID-release of tethered H3.1-mCherry and endogenous EGFP-NASP a stable cell line was used. Partitioning and quantification of the images was carried out using ImageJ. Z-stacks spanning the cell were flattened into a maximum pixel intensity image. The cytosol and nucleus were manually partitioned for each cell, and the nuclear enrichment over the cytosol was calculated for each time point. Values for individual cells were normalised between 1 and 0 and plotted on the same axes for comparison. The Pearson's correlation coefficients between the mCherry (tethered histone) and the EGFP-Imp5 channels were calculated at each time point using the ImageJ JACoP plugin (https://imagej.nih.gov/ij/plugins/track/jacop.html). Values were normalised, taking the last pre-bleach image as 1 and the first post-bleach image as 0. Error bars represent the s.e.m. of six individual experiments.

FRAP

H3.1-/H4-EGFP wild type and mutants (FD, HB) were transfected into HEK293-F cells and seeded onto 8-well µ-slides (ibidi). FRAP experiments were performed using the same confocal microscope as above, equipped with a PhotoKinesis FRAP module. Four pre-bleaching images of a single z-slice were taken before circular regions approximating 2 µm diameter of the cell nucleus were bleached using 30 iterations of the 405 nm laser at 50% power. Images were taken directly after bleaching, and every 15 seconds up to 4 min. Image analysis was perfomed in ImageJ ROI manager to define three areas: 1. bleached area, whole nucleus, and background. Values were normalised, taking the average of pre-bleach images as 1 and the lowest post-bleach image as 0. Error bars represent the s.d. of at least four individual experiments, containing each 2 to 5 bleached cells.

Protein complex prediction

sNASP residues 1-340 and H3 residues 116-135 were used for prediction. AlphaFold2 (Jumper et al., 2021) was run from a Colab notebook using the AlphaFold2-Advanced template (Mirdita et al., 2021). Sequences were used in a 1:1 stoichiometry and treated as separate cahins. The mmSeqs2 method of multiple sequence alignment was implemented.

Acknowledgments

A.J.B and A.J.P are supported by a Wellcome Trust Sir Henry Dale Fellowship (208801/Z/17/Z). Facility support was provided by the Warwick Proteomics Research Technology Platform, CAMDU (Computing and Advanced Microscopy Development Unit), and Warwick Integrative Synthetic Biology (WISB) Centre (for access to flow cytometry facilities). We would like to acknowledge Andrew

Bottill, Cleidi Zampronio and Claire Mitchel for technical support, and colleagues in the Division of Biomedical Sciences at Warwick Medical School for support and advice.

References

Adhikary, S., **Chakravarti, D.**, **Terranova, C.**, **Sengupta, I.**, **Maitituoheti, M.**, **Dasgupta, A.**, **Srivastava, D. K.**, **Ma, J.**, **Raman, A. T.**, **Tarco, E.**, **Sahin, A. A.**, **Bassett, R.**, **Yang, F.**, **Tapia, C.**, **Roy, S.**, **Rai, K.**, and **Das, C.** (2019). Atypical plant homeodomain of UBR7 functions as an H2BK120Ub ligase and breast tumor suppressor. *Nature Communications* **10**, 1398. doi: 10.1038/s41467-019-08986-5.

Alekseev, O. M., **Widgren, E. E.**, **Richardson, R. T.**, and **O'Rand, M. G.** (2005). Association of NASP with HSP90 in mouse spermatogenic cells: stimulation of ATPase activity and transport of linker histones into nuclei. *J Biol Chem* **280**, 2904–2911. doi: 10.1074/jbc.M410397200.

Alvarez, F., **Munoz, F.**, **Schilcher, P.**, **Imhof, A.**, **Almouzni, G.**, and **Loyola, A.** (2011). Sequential establishment of marks on soluble histones h3 and h4. *J Biol Chem* **286**, 17714–17721. doi: 10.1074/jbc.M111.223453.

Apta-Smith, M. J., **Hernandez-Fernaud, J. R.**, and **Bowman, A. J.** (2018). Evidence for the nuclear import of histones H3.1 and H4 as monomers. *The EMBO journal* **37**, e98714. doi: 10.15252/embj.201798714.

Ask, K., **Jasencakova, Z.**, **Menard, P.**, **Feng, Y.**, **Almouzni, G.**, and **Groth, A.** (2012). Codanin-1, mutated in the anaemic disease CDAI, regulates Asf1 function in S-phase histone supply. *EMBO J* **31**, 2013–2023. doi: 10.1038/emboj.2012.55.

Baake, M., **Bauerle, M.**, **Doenecke, D.**, and **Albig, W.** (2001). Core histones and linker histones are imported into the nucleus by different pathways. *Eur J Cell Biol* **80**, 669–677. doi: 10.1078/0171-9335-00208.

Bernardes, N. E. and **Chook, Y. M.** (2020). Nuclear import of histones. *Biochemical Society Transactions* **48**, 2753–2767. doi: 10.1042/BST20200572.

Blackwell Jr., J. S., **Wilkinson, S. T.**, **Mosammaparast, N.**, and **Pemberton, L. F.** (2007). Mutational analysis of H3 and H4 N termini reveals distinct roles in nuclear import. *J Biol Chem* **282**, 20142–20150. doi: 10.1074/jbc.M701989200.

Bowman, A., **Lercher, L.**, **Singh, H. R.**, **Zinne, D.**, **Timinszky, G.**, **Carlomagno, T.**, and **Ladurner, A. G.** (2016). The histone chaperone sNASP binds a conserved peptide motif within the globular core of histone H3 through its TPR repeats. *Nucleic Acids Res* **44**, 3105–3117. doi: 10.1093/nar/gkv1372.

Bowman, A., **Koide, A.**, **Goodman, J. S.**, **Colling, M. E.**, **Zinne, D.**, **Koide, S.**, and **Ladurner, A. G.** (2017). sNASP and ASF1A function through both competitive and compatible modes of histone binding. *Nucleic Acids Res* **45**, 643–656. doi: 10.1093/nar/gkw892.

Campos, E. I. and **Reinberg, D.** (2010). New chaps in the histone chaperone arena. *Genes Dev* **24**, 1334–1338. doi: 10.1101/gad.1946810.

Campos, E. I., **Fillingham, J.**, **Li, G.**, **Zheng, H.**, **Voigt, P.**, **Kuo, W. H.**, **Seepany, H.**, **Gao, Z.**, **Day, L. A.**, **Greenblatt, J. F.**, and **Reinberg, D.** (2010). The program for processing newly synthesized histones H3.1 and H4. *Nat Struct Mol Biol* **17**, 1343–1351. doi: 10.1038/nsmb.1911.

Campos, E. I., **Smits, A. H.**, **Kang, Y. H.**, **Landry, S.**, **Escobar, T. M.**, **Nayak, S.**, **Ueberheide, B. M.**, **Durocher, D.**, **Vermeulen, M.**, **Hurwitz, J.**, and **Reinberg, D.** (2015). Analysis of the Histone H3.1 Interactome: A Suitable Chaperone for the Right Event. *Mol Cell* **60**, 697–709. doi: 10.1016/j.molcel.2015.08.005.

Chook, Y. M. and **Süel, K. E.** (2011). Nuclear import by karyopherin-βs: Recognition and inhibition. *Biochimica et Biophysica Acta (BBA) - Molecular Cell Research* **1813**, 1593–1606. doi: 10.1016/j.bbamcr.2010.10.014.

Cook, A. J., **Gurard-Levin, Z. A.**, **Vassias, I.**, and **Almouzni, G.** (2011). A specific function for the histone chaperone NASP to fine-tune a reservoir of soluble H3-H4 in the histone supply chain. *Mol Cell* **44**, 918–927. doi: 10.1016/j.molcel.2011.11.021.

Ecroyd, H. Redefining the Chaperone Mechanism of sHsps: Not Just Holdase Chaperones. In **Tanguay, R. M.** and **Hightower, L. E.**, editors, *The Big Book on Small Heat Shock Proteins*, Heat Shock Proteins, pages 179–195. Springer International Publishing, Cham, (2015). ISBN 978-3-319-16077-1. URL `https://doi.org/10.1007/978-3-319-16077-1_7`.

English, C. M., **Maluf, N. K.**, **Tripet, B.**, **Churchill, M. E. A.**, and **Tyler, J. K.** (2005). ASF1 binds to a heterodimer of histones H3 and H4: A two-step mechanism for the assembly of the H3-H4 heterotetramer on DNA. *Biochemistry* **44**, 13673–13682.

Evans, R., **O'Neill, M.**, **Pritzel, A.**, **Antropova, N.**, **Senior, A.**, **Green, T.**, **Žídek, A.**, **Bates, R.**, **Blackwell, S.**, **Yim, J.**, **Ronneberger, O.**, **Bodenstein, S.**, **Zielinski, M.**, **Bridgland, A.**, **Potapenko, A.**, **Cowie, A.**, **Tunyasuvunakool, K.**, **Jain, R.**, **Clancy, E.**, **Kohli, P.**, **Jumper, J.**, and **Hassabis, D.** (2021). Protein complex prediction with AlphaFold-Multimer. Technical report. URL `https://www.biorxiv.org/content/10.1101/2021.10.04.463034v1`.

Foltz, D. R., **Jansen, L. E.**, **Bailey, A. O.**, **Yates 3rd, J. R.**, **Bassett, E. A.**, **Wood, S.**, **Black, B. E.**, and **Cleveland, D. W.** (2009). Centromere-specific assembly of CENP-a nucleosomes is mediated by HJURP. *Cell* **137**, 472–484. doi: 10.1016/j.cell.2009.02.039.

Gibson, D. G. (2009). Synthesis of DNA fragments in yeast by one-step assembly of overlapping oligonucleotides. *Nucleic Acids Res* **37**, 6984–6990. doi: 10.1093/nar/gkp687.

Groth, A., **Ray-Gallet, D.**, **Quivy, J. P.**, **Lukas, J.**, **Bartek, J.**, and **Almouzni, G.** (2005). Human Asf1 regulates the flow of S phase histones during replicational stress. *Mol Cell* **17**, 301–311. doi: 10.1016/j.molcel.2004.12.018.

Groth, A., **Corpet, A.**, **Cook, A. J.**, **Roche, D.**, **Bartek, J.**, **Lukas, J.**, and **Almouzni, G.** (2007). Regulation of replication fork progression through histone supply and demand. *Science* **318**, 1928–1931. doi: 10.1126/science.1148992[doi].

Hammond, C. M., **Stromme, C. B.**, **Huang, H.**, **Patel, D. J.**, and **Groth, A.** (2017). Histone chaperone networks shaping chromatin function. *Nat Rev Mol Cell Biol* doi: 10.1038/nrm.2016.159.

Hammond, C. M., **Bao, H.**, **Hendriks, I. A.**, **Carraro, M.**, **García-Nieto, A.**, **Liu, Y.**, **Reverón-Gómez, N.**, **Spanos, C.**, **Chen, L.**, **Rappsilber, J.**, **Nielsen, M. L.**, **Patel, D. J.**, **Huang, H.**, and **Groth, A.** (2021). DNAJC9 integrates heat shock molecular chaperones into the histone chaperone network. *Molecular Cell* **81**, 2533–2548. doi: 10.1016/j.molcel.2021.03.041.

Jakob, U., **Gaestel, M.**, **Engel, K.**, and **Buchner, J.** (1993). Small heat shock proteins are molecular chaperones. *The Journal of Biological Chemistry* **268**, 1517–1520.

Jasencakova, Z., **Scharf, A. N.**, **Ask, K.**, **Corpet, A.**, **Imhof, A.**, **Almouzni, G.**, and **Groth, A.** (2010). Replication stress interferes with histone recycling and predeposition marking of new histones. *Mol Cell* **37**, 736–743. doi: 10.1016/j.molcel.2010.01.033.

Jumper, J., **Evans, R.**, **Pritzel, A.**, **Green, T.**, **Figurnov, M.**, **Ronneberger, O.**, **Tunyasuvunakool, K.**, **Bates, R.**, **Z'idek, A.**, **Potapenko, A.**, **Bridgland, A.**, **Meyer, C.**, **Kohl, S. A. A.**, **Ballard, A. J.**, **Cowie, A.**, **Romera-Paredes, B.**, **Nikolov, S.**, **Jain, R.**, **Adler, J.**, **Back, T.**, **Petersen, S.**, **Reiman, D.**, **Clancy, E.**, **Zielinski, M.**, **Steinegger, M.**, **Pacholska, M.**, **Berghammer, T.**, **Bodenstein, S.**, **Silver, D.**, **Vinyals, O.**, **Senior, A. W.**,

Kavukcuoglu, K., **Kohli, P.**, and **Hassabis, D.** (2021). Highly accurate protein structure prediction with AlphaFold. *Nature* doi: 10.1038/s41586-021-03819-2.

Kleff, S., **Andrulis, E. D.**, **Anderson, C. W.**, and **Sternglanz, R.** (1995). Identification of a gene encoding a yeast histone H4 acetyltransferase. *The Journal of biological chemistry* **270**, 24674–24677. doi: 10.1074/jbc.270.42.24674.

Kleiner, R. E., **Hang, L. E.**, **Molloy, K. R.**, **Chait, B. T.**, and **Kapoor, T. M.** (2018). A Chemical Proteomics Approach to Reveal Direct Protein-Protein Interactions in Living Cells. *Cell Chemical Biology* **25**, 110–120.e3. doi: 10.1016/j.chembiol.2017.10.001.

Lam, S. S., **Martell, J. D.**, **Kamer, K. J.**, **Deerinck, T. J.**, **Ellisman, M. H.**, **Mootha, V. K.**, and **Ting, A. Y.** (2015). Directed evolution of APEX2 for electron microscopy and proximity labeling. *Nat Methods* **12**, 51–54. doi: 10.1038/nmeth.3179.

Lambert, J. P., **Tucholska, M.**, **Go, C.**, **Knight, J. D.**, and **Gingras, A. C.** (2015). Proximity biotinylation and affinity purification are complementary approaches for the interactome mapping of chromatin-associated protein complexes. *J Proteomics* 118, 81–94. doi: 10.1016/j.jprot.2014.09.011.

Li, Y., **Zhang, L.**, **Liu, T.**, **Chai, C.**, **Fang, Q.**, **Wu, H.**, **Agudelo Garcia, P. A.**, **Han, Z.**, **Zong, S.**, **Yu, Y.**, **Zhang, X.**, **Parthun, M. R.**, **Chai, J.**, **Xu, R. M.**, and **Yang, M.** (2014). Hat2p recognizes the histone H3 tail to specify the acetylation of the newly synthesized H3/H4 heterodimer by the Hat1p/Hat2p complex. *Genes Dev* **28**, 1217–1227. doi: 10.1101/gad.240531.114.

Lin, J., **Bao, X.**, and **Li, X. D.** (2021). A tri-functional amino acid enables mapping of binding sites for posttranslational-modification-mediated protein-protein interactions. *Molecular Cell* doi: 10.1016/j.molcel.2021.04.001.

Luger, K., **Rechsteiner, T. J.**, **Flaus, A. J.**, **Waye, M. M. Y.**, and **Richmond, T. J.** (1997). Characterization of nucleosome core particles containing histone proteins made in bacteria. *Journal of Molecular Biology* **272**, 301–311.

McClelland, S. E. and **McAinsh, A. D.** Hydrodynamic Analysis of Human Kinetochore Complexes During Mitosis. In **McAinsh, A. D.**, editor, *Mitosis: Methods and Protocols*, Methods in Molecular Biology, pages 81–98. Humana Press, Totowa, NJ, (2009). ISBN 978-1-60327-993-2. URL `https://doi.org/10.1007/978-1-60327-993-2_5`.

Mirdita, M., **Ovchinnikov, S.**, and **Steinegger, M.** (2021). ColabFold - Making protein folding accessible to all. preprint, Bioinformatics. URL `http://biorxiv.org/lookup/doi/10.1101/2021.08.15.456425`.

Mogk, A. and **Bukau, B.** (2017). Role of sHsps in organizing cytosolic protein aggregation and disaggregation. *Cell Stress & Chaperones* **22**, 493–502. doi: 10.1007/s12192-017-0762-4.

Mosammaparast, N., **Jackson, K. R.**, **Guo, Y.**, **Brame, C. J.**, **Shabanowitz, J.**, **Hunt, D. F.**, and **Pemberton, L. F.** (2001). Nuclear import of histone H2A and H2B is mediated by a network of karyopherins. *Journal of Cell Biology* **153**, 251–262.

Mosammaparast, N., **Guo, Y.**, **Shabanowitz, J.**, **Hunt, D. F.**, and **Pemberton, L. F.** (2002). Pathways mediating the nuclear import of histones H3 and H4 in yeast. *J Biol Chem* **277**, 862–868. doi: 10.1074/jbc.M106845200.

Muhlhausser, P., **Muller, E. C.**, **Otto, A.**, and **Kutay, U.** (2001). Multiple pathways contribute to nuclear import of core histones. *EMBO Rep* **2**, 690–696. doi: 10.1093/embo-reports/kve168.

Murzina, N. V., **Pei, X. Y.**, **Zhang, W.**, **Sparkes, M.**, **Vicente-Garcia, J.**, **Pratap, J. V.**, **McLaughlin, S. H.**, **Ben-Shahar, T. R.**, **Verreault, A.**, **Luisi, B. F.**, and **Laue, E. D.** (2008). Structural basis for the recognition of histone H4 by the histone-chaperone RbAp46. *Structure* **16**, 1077–1085. doi: https://doi.org/10.1016/j.str.2008.05.006.

Mymrikov, E. V., **Daake, M.**, **Richter, B.**, **Haslbeck, M.**, and **Buchner, J.** (2017). The Chaperone Activity and Substrate Spectrum of Human Small Heat Shock Proteins. *The Journal of Biological Chemistry* **292**, 672–684. doi: 10.1074/jbc.M116.760413.

Natsume, R., **Eitoku, M.**, **Akai, Y.**, **Sano, N.**, **Horikoshi, M.**, and **Senda, T.** (2007). Structure and function of the histone chaperone CIA/ASF1 complexed with histones H3 and H4. *Nature* **446**, 338–341.

O'Rand, M. G., **Richardson, R. T.**, **Zimmerman, L. J.**, and **Widgren, E. E.** (1992). Sequence and localization of human NASP: conservation of a Xenopus histone-binding protein. *Dev Biol* **154**, 37–44. doi: 0012-1606(92)90045-I[pii].

Padavannil, A., **Sarkar, P.**, **Kim, S. J.**, **Cagatay, T.**, **Jiou, J.**, **Brautigam, C. A.**, **Tomchick, D. R.**, **Sali, A.**, **D'Arcy, S.**, and **Chook, Y. M.** (2019). Importin-9 wraps around the H2A-H2B core to act as nuclear importer and histone chaperone. *eLife* 8, e43630. doi: 10.7554/eLife.43630.

Pardal, A., **Fernandes-Duarte, F.**, and **Bowman, A.** (2019). The histone chaperoning pathway: from ribosome to nucleosome. *Essays in Biochemistry* **63**, 29–43. doi: 10.1042/EBC20180055.

Ran, F. A., **Hsu, P. D.**, **Wright, J.**, **Agarwala, V.**, **Scott, D. A.**, and **Zhang, F.** (2013). Genome engineering using the CRISPR-Cas9 system. *Nature Protocols* **8**, 2281–2308. doi: 10.1038/nprot.2013.143.

Reinle, K., **Mogk, A.**, and **Bukau, B.** (2021). The Diverse Functions of Small Heat Shock Proteins in the Proteostasis Network. *Journal of Molecular Biology* page 167157. doi: 10.1016/j.jmb.2021.167157.

Shevchenko, A., **Tomas, H.**, **Havli, J.**, **Olsen, J. V.**, and **Mann, M.** (2006). In-gel digestion for mass spectrometric characterization of proteins and proteomes. *Nature Protocols* **1**, 2856–2860. doi: 10.1038/nprot.2006.468.

Smith, S. and **Stillman, B.** (1989). Purification and characterization of CAF-I, a human cell factor required for chromatin assembly during DNA replication in vitro. *Cell* **58**, 15–25. doi: 10.1016/0092-8674(89)90398-x.

Song, J. J., **Garlick, J. D.**, and **Kingston, R. E.** (2008). Structural basis of histone H4 recognition by p55. *Genes Dev* **22**, 1313–1318. doi: gad.1653308[pii]10.1101/gad.1653308[doi].

Soniat, M., **Cagatay, T.**, and **Chook, Y. M.** (2016). Recognition Elements in the Histone H3 and H4 Tails for Seven Different Importins. *J Biol Chem* **291**, 21171–21183. doi: 10.1074/jbc.M116.730218.

Suzuki, K., **Bose, P.**, **Leong-Quong, R. Y.**, **Fujita, D. J.**, and **Riabowol, K.** (2010). REAP: A two minute cell fractionation method. *BMC Res Notes* 3, 294. doi: 10.1186/1756-0500-3-294.

Tagami, H., **Ray-Gallet, D.**, **Almouzni, G.**, and **Nakatani, Y.** (2004). Histone H3.1 and H3.3 complexes mediate nucleosome assembly pathways dependent or independent of DNA synthesis. *Cell* **116**, 51–61.

Taipale, M., **Tucker, G.**, **Peng, J.**, **Krykbaeva, I.**, **Lin, Z.-Y.**, **Larsen, B.**, **Choi, H.**, **Berger, B.**, **Gingras, A.-C.**, and **Lindquist, S.** (2014). A quantitative chaperone interaction network reveals the architecture of cellular protein homeostasis pathways. *Cell* **158**, 434–448. doi: 10.1016/j.cell.2014.05.039.

Tyanova, S., **Temu, T.**, and **Cox, J.** (2016). The MaxQuant computational platform for mass spectrometry-based shotgun proteomics. *Nature Protocols* **11**, 2301–2319. doi: 10.1038/nprot.2016.136.

Tyler, J. K., **Adams, C. R.**, **Chen, S. R.**, **Kobayashi, R.**, **Kamakaka, R. T.**, and **Kadonaga, J. T.** (1999). The RCAF complex mediates chromatin assembly during DNA replication and repair. *Nature* **402**, 555–560.

Verreault, A., **Kaufman, P. D.**, **Kobayashi, R.**, and **Stillman, B.** (1998). Nucleosomal DNA regulates the core-histone-binding subunit of the human Hat1 acetyltransferase. *Curr Biol* **8**, 96–108.

Wu, H., **Moshkina, N.**, **Min, J.**, **Zeng, H.**, **Joshua, J.**, **Zhou, M. M.**, and **Plotnikov, A. N.** (2012). Structural basis for substrate specificity and catalysis of human histone acetyltransferase 1. *Proc Natl Acad Sci U S A* **109**, 8925–8930. doi: 10.1073/pnas.1114117109.

Yoon, J., **Kim, S. J.**, **An, S.**, **Cho, S.**, **Leitner, A.**, **Jung, T.**, **Aebersold, R.**, **Hebert, H.**, **Cho, U.-S.**, and **Song, J.-J.** (2018). Integrative Structural Investigation on the Architecture of Human Importin4_histone H3/H4_asf1a Complex and Its Histone H3 Tail Binding. *Journal of Molecular Biology* **430**, 822–841. doi: 10.1016/j.jmb.2018.01.015.